

Surface Dislocation Nucleation Mediated Deformation and Ultrahigh Strength in Sub-10-nm Gold Nanowires

Yang Lu^{1†}, Jun Song², Jian Yu Huang³, and Jun Lou¹ (✉)

¹ Department of Mechanical Engineering & Materials Science, Rice University, Houston, TX 77005, USA

² Department of Mining & Materials Engineering, McGill University, Montreal, QC H3A 2B2, Canada

³ Center for Integrated Nanotechnologies (CINT), Sandia National Laboratories, Albuquerque, NM 87185, USA

[†] Present address: Department of Materials Science and Engineering, MIT, Cambridge, MA 02139, USA

Received: 4 April 2011 / Revised: 29 September 2011 / Accepted: 4 October 2011

© Tsinghua University Press and Springer-Verlag Berlin Heidelberg 2011

ABSTRACT

The plastic deformation and the ultrahigh strength of metals at the nanoscale have been predicted to be controlled by surface dislocation nucleation. *In situ* quantitative tensile tests on individual <111> single crystalline ultrathin gold nanowires have been performed and significant load drops observed in stress–strain curves suggest the occurrence of such dislocation nucleation. High-resolution transmission electron microscopy (HRTEM) imaging and molecular dynamics simulations demonstrated that plastic deformation was indeed initiated and dominated by surface dislocation nucleation, mediating ultrahigh yield and fracture strength in sub-10-nm gold nanowires.

KEYWORDS

Nanowires, *in situ* transmission electron microscope (TEM), mechanical characterization, dislocation nucleation, plasticity

1. Introduction

Size-dependent plasticity and fracture behavior of one-dimensional metallic nanowires offer exciting potential ways of revealing fundamental mechanisms of deformation and failure, as the length scale of metals approaches atomic spacing. Uni-axial compression of focus ion beam machined single crystalline metallic pillars with diameters of tens of micrometers to hundreds of nanometers showed strong size effects with much higher yield stress for smaller pillars without the presence of strain gradients [1, 2]. A conceptual framework of “dislocation starvation” [1] was proposed to be responsible for this apparent size-dependent behavior. The “mechanical annealing” phenomena [3]

observed by means of a transmission electron microscope (TEM) during compression of Ni pillars suggests that gliding dislocation could leave a crystal more rapidly than it multiplies, which leads to a dislocation-starved state requiring very high stress to nucleate new mobile dislocations in such a small crystal volume. When the crystal size is further reduced to tens of nanometers and below, surface dislocation nucleation has been predicted to play a more critical role in controlling plastic deformation and subsequent fracture behavior [4, 5]. Unfortunately, experimental evidence for such surface dislocation nucleation aspects of small-scale plasticity, which requires careful quantitative *in situ* investigations, remains elusive.

Early studies of quantitative mechanical testing of

Address correspondence to jlou@rice.edu



one-dimensional (1-D) nanostructures were primarily carried out *ex situ*, using techniques such as nanoindentation [1], resonant oscillation [6], and atomic force microscopy (AFM) deflection [7] tests. These generally lack real time structural monitoring, and do not permit a one-to-one correlation between mechanical data and internal structural evolution. Recently, *in situ* mechanical characterization of individual nanowires with diameters from tens to hundreds of nanometers inside a TEM were realized under various loading geometries, such as bending [8], buckling [9], and compression [3]. However, use of the most efficient and easy-to-interpret tensile testing method for measuring intrinsic mechanical properties of exceedingly small nanowire samples inside a TEM poses significant challenges due to difficulties associated with sample clamping, alignment and accurate measurements of load and displacement. Researchers have developed various microelectromechanical systems (MEMS) devices to perform *in situ* tensile tests on metallic (e.g., Au, Pd, Ni) nanowires and carbon nanotubes [10–14], biological fibrils [15], and nanoscale gold thin films [16]. However, the diameters of the nanowires tested using MEMS stages were usually in the range of tens or hundreds of nanometers. In order to test metallic nanowires with sub-10-nm diameters, it is necessary to prepare samples *in situ* by using either the mechanically

controllable break junction technique (MCBJT) [17] or the nanometer tip–substrate [18]/tip–tip [19] contact-then-withdraw techniques to form nanosized metal samples. Unfortunately the crystalline structure and orientation of samples previously prepared by these methods were not well-controlled, and sample diameters were non-uniform (ranging from a few angstroms to a few microns). These drawbacks have hindered quantitative characterization and understanding of the deformation and fracture mechanisms for metals at the sub-10-nm scale, despite some recent efforts to qualitatively study detailed plasticity mechanisms in sub-10-nm-sized Au crystals [20].

In this paper, we present results of *in situ* quantitative tensile tests of gold nanowires with diameters of less than 10 nm. Rather than pulling randomly formed nanosized gold samples, we successfully clamped individual pre-fabricated free-standing nanowires with well-controlled crystalline structures and orientations onto the AFM cantilever which acted as the force sensor, and performed quantitative tensile tests directly inside a high-resolution TEM (HRTEM) (Figs. 1(a)–1(d)). Ultrathin gold nanowires with uniform diameters ranging from 7 to 10 nm were used (Fig. 1(e)) in this study and were chemically synthesized by the reduction of HAuCl_4 in oleic acid (OA) and oleylamine (OAm) [21]. These high-aspect-ratio nanowires had lengths

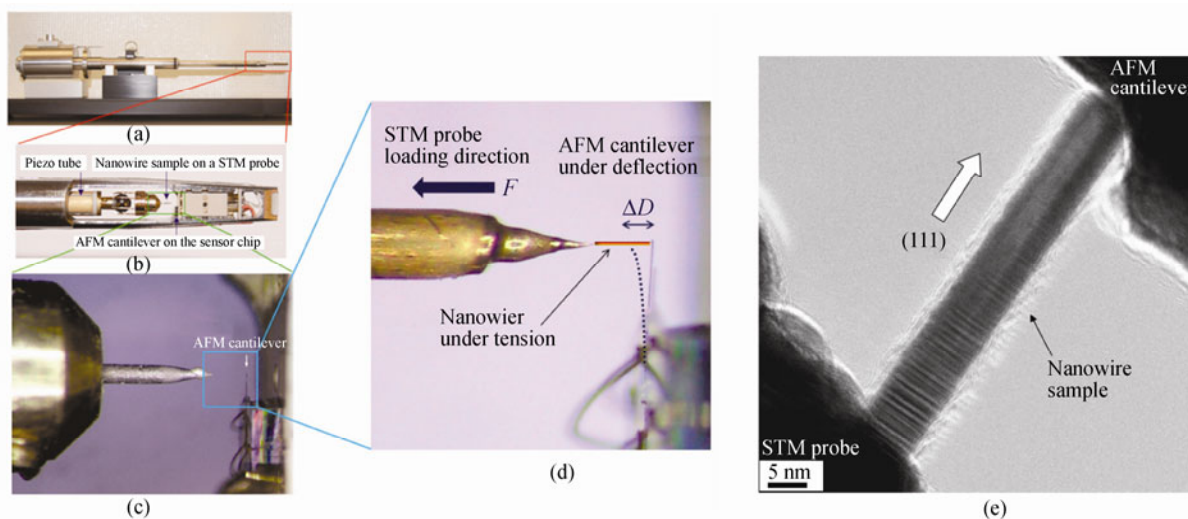


Figure 1 Experimental set-up and materials preparation: (a) the Nanofactory™ TEM–AFM holder; (b) image and (c) zoom-in image showing the holder configuration; (d) illustration of the quantitative testing configuration with the AFM cantilever as the force sensor; (e) HRTEM image of a 7 nm nanowire showing the lattice fringes, indicating that the nanowire grows along the $\langle 111 \rangle$ direction

ranging from tens of nanometers up to a few microns. They were also verified to be single crystal in the $\langle 111 \rangle$ growth direction, with measured average lattice fringe spacings of ~ 0.23 nm (corresponding to the $\{111\}$ lattice spacing of gold) from their HRTEM images (Fig. 1(e)). Quantitative tensile tests were conducted by using a Nanofactory™ TEM–AFM sample holder (Fig. 1(a)) and experimental details are described below.

2. Experimental

The TEM samples were prepared by adhering ultrathin gold nanowires onto a gold or tungsten scanning tunneling microscope (STM) probe using conductive silver glue. Then the STM probe with attached Au nanowires was loaded into the Nanofactory™ TEM–AFM sample holder (Fig. 1(a)) and manipulated by a piezo-driven head (Figs. 1(b) and 1(c)). The sample clamping was facilitated by coating the tip of the silicon AFM cantilever with a thin (tens of nanometers) adhesive layer of nanoscale amorphous silica, functioning as a “glue” [22]. During tensile tests, an AFM cantilever beam with known spring constant $k = 4.8$ N/m was deflected by an individual nanowire sample pulled by the piezo tube in displacement control mode (Fig. 1(d)). Sample elongation and the change in diameter were monitored directly via real time TEM imaging and the force was calculated by the recorded deflection of the AFM cantilever. A linear relationship was assumed between the deflection and force ($F = k \times \Delta D$), considering the small deflections involved. A stationary e-beam-blocking bar was inserted as a reference marker for all displacement measurements. All experiments were performed inside a FEI™ Tecnai G² F30 HRTEM, operated at 300 kV working voltage. It is also worth noting that no current was passed through the samples and very low dose electron beams (~ 1 A/cm²) were used in order to reduce the electron irradiation-induced heating in all the experiments.

3. Results and discussion

3.1 *In situ* TEM quantitative tensile tests

In Figs. 2(a)–2(e), an ultrathin Au nanowire (diameter ~ 10 nm and length ~ 70 nm) was deformed and

fractured under tensile loading (see Movie S-1 in the Electronic Supplementary Material (ESM)). Figure 2(f) shows the corresponding engineering stress and strain data obtained by measuring cantilever deflections and sample elongations. The nanowire experienced an impressive $\sim 26\%$ total engineering strain before final failure. During plastic deformation, the nanowire kept necking down to a point and formed atom chains at the final stage right before fracture (Movie S-1 in the ESM). Since the actual instantaneous diameter of the deforming nanowires could be measured using HRTEM during tensile tests, the true stress versus strain curve (Fig. 2(g)) was also obtained. Clear size effects on fracture strength were observed for ultrathin Au nanowires, with an engineering fracture strength of ~ 620 MPa—much higher than the fracture strength of bulk gold (~ 100 MPa [23]). Taking into consideration the dramatic reduction in cross-section area due to necking, the corresponding true fracture strength was estimated to be ~ 7 GPa. This value is very close to the ideal strength of a gold crystal (~ 8 GPa [24]), and higher than most of the reported experimental strength data (ranging from 0.8–6 GPa) for Au nanowires with larger diameters [7, 24]. This true fracture strength value is also comparable to the experimentally measured strength of a single Au atomic chain (~ 13 GPa) [25], owing to the extensive necking process experienced by the Au nanowire before fracture.

More interestingly, very significant load drop was observed in the stress–strain curve (Fig. 2(f)) after the initial elastic deformation, where the engineering stress of the Au nanowire dropped from ~ 1.1 GPa down to ~ 460 MPa. The measured yield stress of ~ 1.1 GPa is extremely high for Au, comparable to theoretical prediction of the ideal shear strength from density functional theory (DFT) calculations, i.e., 850 MPa–1.4 GPa, depending on the loading mode [26]. The ultrahigh yield strength of the ultrathin gold nanowire can be attributed to the lack of pre-existing mobile dislocations in the ultrasmall nanowire (Figs. 2(a) and 3(a)) [24]. Furthermore, the stress drop was quite abrupt and did not seem to be a random event, as a similar load drop was also observed in another quantitative tensile test of a similar Au nanowire (see Movie S-2 and associated material in the ESM). It is believed that the large load drop is associated with



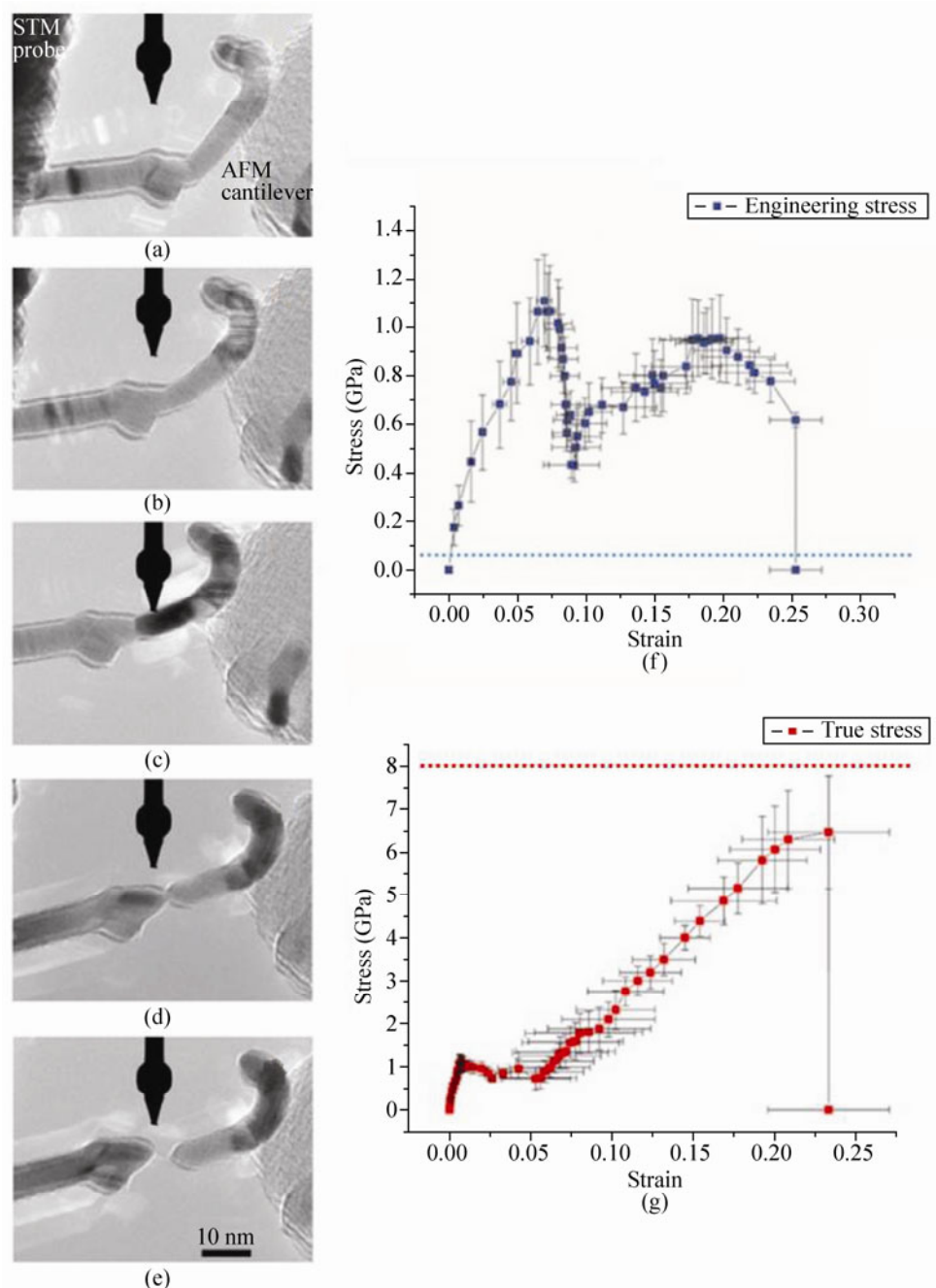


Figure 2 Image frames (a)–(e) showing a quantitative tensile test of a gold nanowire with diameter ~ 10 nm (scale bar 10 nm); corresponding (f) engineering and (g) true stress versus strain curves for the test shown in (a)–(e); error bars were obtained by multiple measurements from nanowire lengths and AFM cantilever deflections, as well as the imaging area movement corrections. The blue line in (f) indicates the fracture strength (~ 100 MPa, [23]) of bulk gold, and the red line in (g) indicates the theoretical strength of gold (~ 8 GPa [24])

the onset and rapid succession of multiple dislocation activities, including nucleation and subsequent slip propagation across the nanowire (Figs. 3 and 4 and associated material in the ESM). The significant load-drops in uni-axial stress–strain curves could be

better observed experimentally if the initial sample was nearly dislocation free; this was achieved either by fabrication or “mechanical annealing” processes. Thus our experiments provide direct evidence for the predicted load drop in nanowire tensile tests.

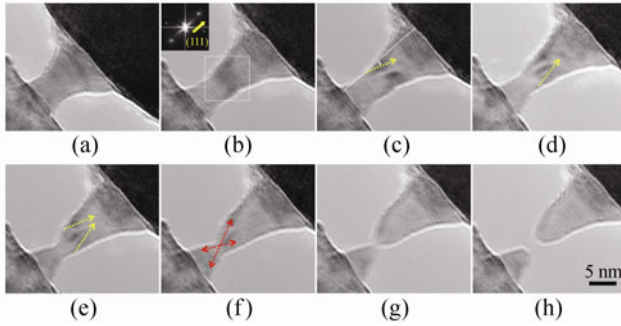


Figure 3 HRTEM images of a short gold nanowire under tensile testing (a)–(h) (scale bar 5 nm): after the elastic deformation region (a)–(b), initial surface dislocation nucleation is indicated by the arrow in (c) with the approximate edge profile of the nanowire marked by the dotted line. Arrows in (d)–(f) indicate more similar surface dislocations emitted from both sides of the nanowire surfaces, and a neck (e)–(g) was formed in the middle section of the nanowire until the final fracture occurred as shown in (h). The insert in (b) shows a fast Fourier transform (FFT) image calculated from the image inside the white square, showing the wire orientation

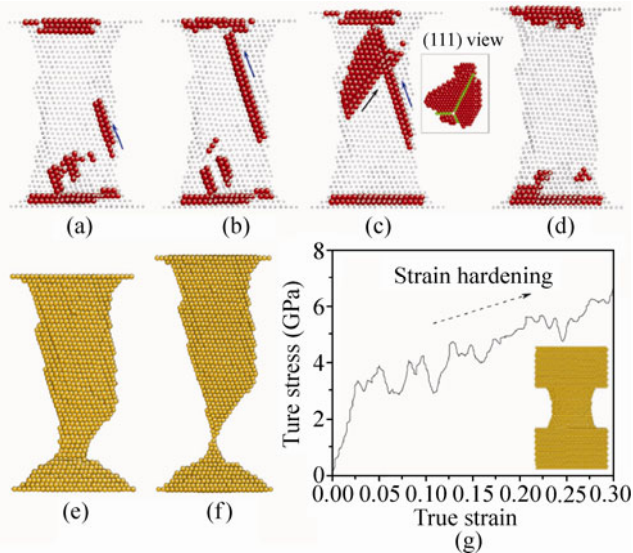


Figure 4 Dislocation activities observed during the deformation of a Au nanowire in MD simulations. (a) Nucleation of a Shockley partial dislocation from the surface. (b) The nucleated surface partial dislocation propagates into the bulk. (c) Another Shockley partial dislocation nucleates from the surface, propagates across the nanowire and intersects the previously nucleated Shockley partial dislocation. The intersection creates stair-rod segments, as indicated in the small inserted figure (projection view along the [111] direction) with atoms in stair-rods colored green). (d) Further loading leads to the annihilation of dislocations, leaving the nanowire with a nearly perfect crystalline structure. (e) and (f) Final sample morphology including the atomic chain observed immediately before the final fracture. (g) The corresponding true stress and strain curve (the insert shows the original sample morphology). Figures (a)–(d) are the cross-sectional views of the nanowire, with only surface atoms (red) and atoms in stacking faults shown for clarity. Figures (e) and (f) are the projection views of all atoms in the nanowire along the $[1\bar{1}0]$ direction

3.2 *In situ* HRTEM tensile tests

To fully reveal the underlying deformation mechanisms associated with the observed significant load drop phenomenon, and specifically the exact location of the dislocation nucleation event, tensile tests in HRTEM mode were performed using a shorter nanowire in order to ensure high quality imaging of the deforming region. Figures 3(a)–3(h) show the deformation process of a single crystalline gold nanowire (~30 nm in initial length) with the same $\langle 111 \rangle$ growth orientation (see Movie S-3 in the ESM). The loading rate was slightly slower to give better image quality (at ~0.2 nm/s and strain rate ~0.001/s). The sample was pulled in the same uni-axial loading direction along the $\langle 111 \rangle$ nanowire axis. The nanowire first experienced an elastic deformation region with no apparent lattice structural change (Figs. 3(a) and 3(b)), which correlates well with the earlier quantitatively measured elastic strain of a few percent (Fig. 2(f)). The onset of the plastic deformation was indicated by the sudden appearance of a dislocation slip trace apparently emitted from the nanowire surface, as marked in Fig. 3(c) (see also Movie S-3 in the ESM). Due to the extremely small sample volume available, the nucleated dislocations are thought to slip swiftly across the nanowire. By measuring the angle between the slip trace and the wire axis (~19.5° as shown in Fig. 3(c)), it was confirmed that the dislocation slip occurred on another {111} plane. With further deformation, additional similar dislocations were emitted from both sides of the nanowire surfaces and then slipped quickly across the nanowire along intersecting {111} planes to gradually form a necked region in the middle section of the nanowire (Figs. 3(d)–3(g)). The neck kept reducing its thickness, with nucleated surface dislocations continuously exiting the nanowire along the corresponding slip planes, giving rise to extensive plastic deformation and a significant reduction in cross-section area leading to the final fracture of the nanowire.

3.3 MD simulations

To better understand the deformation mechanisms observed in the experiments, molecular dynamics simulations employing the embedded-atom method potential developed by Cai and Ye (CY EAM) were performed [27]. The CY EAM potential is a widely



used potential that offers reasonable descriptions of interatomic forces, bulk properties and surface phenomena. Besides the CY potential, preliminary studies using other potentials, e.g., the EAM potentials developed by Mei et al. [28] and Grochola et al. [29], were also conducted for comparison and verification, and qualitative agreement between simulation results was observed.

The atomic configuration of the system is shown in Fig. S-2(a) (in the ESM), where a nanowire of length 5.2 nm and a minimum diameter $D = 5$ nm is sandwiched between two substrates. Note here the nanowire is not strictly cylindrical, but rather a curved shape is used to give better welding between the nanowire and substrates. The curved shape ensures that the initiation of plastic deformation occurs near the center of the nanowire, and not at the locations where it welds to the substrates, thus minimizing any effects the substrates may introduce. The system was equilibrated at $T = 300$ K. The nanowire was then deformed using a pulling velocity of 0.5 m/s, resulting in a tensile force F_z on the nanowire. Simulations using lower straining rates (as low as 0.01 m/s) were also performed, and almost identical results were obtained. Typical dislocation activities observed in the simulations are plotted in Figs. 4(a)–4(d). From the simulations we can explicitly see partial dislocation nucleating from the nanowire surface and propagating into the material, and the cross-over of two partial dislocations. These are the exact features observed experimentally (Figs. 3(c)–3(f)), although not at such high resolution. This was then followed by necking of the nanowire to an atomic chain before final fracture at a stress level close to theoretical strength (Figs. 4(e)–4(g)), again similar to earlier experimental observations (Figs. 2(g), 3(g) and 3(h) and Movie S-3 in the ESM). Simulated true stress and strain curves are also plotted in Fig. 4(g). Significant load drops and apparent work hardening as observed experimentally (Fig. 2(g)) were clearly present. The intriguing work hardening is probably mostly controlled by the diameter-dependent nucleation stress of surface dislocation loops. The smaller the nanowire diameter caused by the necking process, the higher the stress required to nucleate new surface dislocations to sustain the plastic deformation, giving rise to the observed hardening behavior (as shown in the ESM). When the nanowire diameter drops below a critical

value, surface dislocations cease to nucleate as observed in the simulations (Figs. 4(e) and 4(f)), resulting in sample fractures at a stress level close to the theoretical strength (Figs. 2(g) and 4(g)).

4. Conclusions

In summary, ultrahigh yield and fracture strength close to theoretical predictions were measured in $\langle 111 \rangle$ oriented single crystalline Au nanowires with sub-10-nm diameters. Quantitative *in situ* tensile experiments inside a HRTEM and corresponding MD simulations unambiguously revealed the underlying processes of necking formation and subsequent fracture mediated by surface dislocation nucleation in ultrathin gold nanowires. The direct observation of this unique mechanism confirms the long expected, but rarely experimentally verified, critical roles played by surface dislocation nucleation in plasticity and fracture of metal nanowires.

Acknowledgements

The authors acknowledge the financial support provided by the Air Force Office of Sponsored Research (AFOSR) YIP award FA9550-09-1-0084, by the Welch Foundation grant C-1716 and by the National Science Foundation (NSF) grant No. DMR-1128818. This work was performed, in part, at the Center for Integrated Nanotechnologies, a U.S. Department of Energy, Office of Basic Energy Sciences user facility at Los Alamos National Laboratory (Contract DE-AC52-06NA25396) and Sandia National Laboratories (Contract DE-AC04-94AL85000). Sandia National Laboratories is a multi-program laboratory operated by Sandia Corporation, a wholly-owned subsidiary of Lockheed Martin Corporation, for the U.S. Department of Energy's National Nuclear Security Administration under contract DE-AC04-94AL85000. The authors also thank Prof. Shouheng Sun from Brown University for providing ultrathin gold nanowire samples and Dr. Wenhua Guo at Rice University for discussions about the TEM analysis.

Electronic Supplementary Material: Supplementary material (additional quantitative experiments at low magnification; further discussions of load drops,

character of dislocations, and work hardening mechanisms; supplementary movies) is available in the online version of this article at <http://dx.doi.org/10.1007/s12274-011-0177-y>.

References

- [1] Greer, J. R.; Nix, W. D. Nanoscale gold pillars strengthened through dislocation starvation. *Phys. Rev. B* **2006**, *73*, 245410.
- [2] Uchic, M. D.; Dimiduk, M. D.; Florando, J. N.; Nix, W. D. Sample dimensions influence strength and crystal plasticity. *Science* **2004**, *305*, 986–989.
- [3] Shan, Z. W.; Mishra, R. K.; Asif, S. A. S.; Warren, O. L.; Minor, A. M. Mechanical annealing and source-limited deformation in submicrometre-diameter Ni crystals. *Nat. Mater.* **2008**, *7*, 115–119.
- [4] Rabkin, E.; Srolovitz, D. J. Onset of plasticity in gold nanopillar compression. *Nano Lett.* **2007**, *7*, 101–107.
- [5] Zhu, T.; Li, J.; Samanta, A.; Leach, A.; Gall, K. Temperature and strain rate dependence of surface dislocation nucleation. *Phys. Rev. Lett.* **2008**, *100*, 025502.
- [6] Cimalla, V.; Röhligh, C. C.; Pezoldt, J.; Niebelschütz, M.; Ambacher, O.; Brückner, K.; Hein, M.; Weber, J.; Milenkovic, S.; Smith, A. J.; Hassel, A. W. Nanomechanics of single crystalline tungsten nanowires. *J. Nanomater.* **2008**, *2008*, 638947.
- [7] Wu, B.; Heidelberg, A.; Boland, J. J. Mechanical properties of ultrahigh-strength gold nanowires. *Nat. Mater.* **2005**, *4*, 525–529.
- [8] Wang, M. S.; Kaplan-Ashiri, I.; Wei, X.; Rosentsveig, R.; Wagner, H.; Tenne, R.; Peng, L. *In situ* TEM measurements of the mechanical properties and behavior of WS₂ nanotubes. *Nano Res.* **2008**, *1*, 22–31.
- [9] Hsin, C. L.; Mai, W. J.; Gu, Y. D.; Gao, Y. F.; Huang, C. T.; Liu, Y. Z.; Chen, L. J.; Wang, Z. L. Elastic properties and buckling of silicon nanowires. *Adv. Mater.* **2008**, *20*, 3919–3923.
- [10] Zhu, Y.; Moldovan, N.; Espinosa, H. D. A microelectromechanical load sensor for *in situ* electron and X-ray microscopy tensile testing of nanostructures. *Appl. Phys. Lett.* **2005**, *86*, 013506.
- [11] Zhu, Y.; Espinosa, H. D. An electromechanical material testing system for *in situ* electron microscopy and applications. *Proc. Natl. Acad. Sci. U.S.A.* **2005**, *102*, 14503–14508.
- [12] Peng, B.; Locascio, M.; Zapol, P.; Li, S. Y.; Mielke, S. L.; Schatz, G. C.; Espinosa, H. D. Measurements of near-ultimate strength for multiwalled carbon nanotubes and irradiation-induced crosslinking improvements. *Nat. Nanotechnol.* **2008**, *3*, 626–631.
- [13] Lu, Y.; Ganesan, Y.; Lou, J. A multi-step method for *in situ* mechanical characterization of 1-D nanostructures using a novel micromechanical device. *Exp. Mech.* **2010**, *50*, 47–54.
- [14] Ganesan, Y.; Lu, Y.; Peng, C.; Lu, H.; Ballarini, R.; Lou, J. Development and application of a novel microfabricated device for the *in situ* tensile testing of 1-D nanomaterials. *J. Microelectromech. Syst.* **2010**, *19*, 675–682.
- [15] Eppell, S. J.; Smith, B. N.; Kahn, H.; Ballarini, R. Nano measurements with micro-devices: Mechanical properties of hydrated collagen fibrils. *J. R. Soc. Interface* **2006**, *3*, 117–121.
- [16] Haque, M. A.; Saif, M. T. A. Deformation mechanisms in free-standing nanoscale thin films: A quantitative *in situ* transmission electron microscope study. *Proc. Natl. Acad. Sci. U.S.A.* **2004**, *101*, 6335–6340.
- [17] Guo, H.; Yan, P. F.; Wang, Y. B.; Tan, J.; Zhang, Z. F.; Sui, M. L.; Ma, E. Tensile ductility and necking of metallic glass. *Nat. Mater.* **2007**, *6*, 735–739.
- [18] Agrait, N.; Rubio, G.; Vieira, S. Plastic deformation of nanometer-scale gold connective necks. *Phys. Rev. Lett.* **1995**, *74*, 3995–3998.
- [19] Kizuka, T. Atomistic visualization of deformation in gold. *Phys. Rev. B* **1998**, *57*, 11158–11163.
- [20] Zheng, H.; Cao, A. J.; Weinberger, C. R.; Huang, J. Y.; Du, K.; Wang, J. B.; Ma, Y.; Xia, Y. N.; Mao, S. X. Discrete plasticity in sub-10-nm-sized gold crystals. *Nat. Commun.* **2010**, *1*, 1–8.
- [21] Wang, C.; Hu, Y. J.; Lieber, C. M.; Sun, S. H. Ultrathin Au nanowires and their transport properties. *J. Am. Chem. Soc.* **2008**, *130*, 8902–8903.
- [22] Zheng, K.; Wang, C. C.; Cheng, Y. Q.; Yue, Y. H.; Han, X. D.; Zhang, Z.; Shan, Z. W.; Mao, S. X.; Ye, M. M.; Yin, Y. D.; Ma, E. Electron-beam-assisted superplastic shaping of nanoscale amorphous silica. *Nat. Commun.* **2010**, *1*, 1–8.
- [23] Howatson, A. M.; Lund, P. G.; Todd, J. D. *Engineering Tables and Data*, 2nd ed.; Chapman and Hall: London, 1991; p 41.
- [24] Zhu, T.; Li, J.; Ogata, S.; Yip, S. Mechanics of ultra-strength materials. *MRS Bull.* **2009**, *34*, 167–172.
- [25] Rubio-Bollinger, G.; Bahn, S. R.; Agrait, N.; Jacobsen, K. W.; Vieira, S. Mechanical properties and formation mechanisms of a wire of single gold atoms. *Phys. Rev. Lett.* **2001**, *87*, 026101.
- [26] Ogata, S.; Li, J.; Hirotsuki, N.; Shibutani, Y.; Yip, S. Ideal shear strain of metals and ceramics. *Phys. Rev. B* **2004**, *70*, 104104.
- [27] Cai, J.; Ye, Y. Y. Simple analytical embedded-atom-potential model including a long-range force for fcc metals and their alloys. *Phys. Rev. B* **1996**, *54*, 8398–8410.
- [28] Mei, J.; Davenport, J. W.; Fernando, G. W. Analytic embedded-atom potentials for fcc metals—application to liquid and solid copper. *Phys Rev B* **1991**, *43*, 4653–4658.
- [29] Grochola, G.; Russo, S. P.; Snook, I. K. On fitting a gold embedded atom method potential using the force matching method. *J. Chem. Phys.* **2005**, *123*, 204719.

